Discrete self-trapping, soliton interactions, and beam steering in nonlinear waveguide arrays

A. B. Aceves
Department of Mathematics and Statistics, University of New Mexico, Albuquerque, New Mexico 87131

C. De Angelis*
Dipartimento di Elettronica e Informatica, Universita' di Padova, Via Gradenigo 6/a, 35131 Padova, Italy

T. Peschel, R. Muschall, and F. Lederer
University of Jena, Faculty of Physics and Astronomy, Max-Wien-Platz 1, 07743 Jena, Germany

S. Trillo and S. Wabnitz
Fondazione Ugo Bordoni, Via B. Castiglione 59, 00142 Rome, Italy
(Received 16 June 1995)

We investigate the self-trapping phenomenon in one-dimensional nonlinear waveguide arrays. We discuss various approximate analytical descriptions of the discrete self-trapped solutions. We analyze the packing, steering, and collision properties of these solutions, by means of a variational approach and soliton perturbation theory. We compare the analytical and numerical results.

PACS number(s): 42.81.Qb, 42.65.Tg, 63.20.Pw, 46.10.+z

I. INTRODUCTION

Arrays of passive or active coupled optical waveguides may be employed for several device applications [1–5]. In nonlinear waveguide or fiber arrays (NFA's), the characteristics of the device may be tuned by the input power of the beam, which permits ultrafast all-optical switching, as it was first proposed for a passive two-guide coupler in Refs. [6,7]. An interesting property of linearly coupled nonlinear waveguide systems, which originates from the coherent nature of the propagating electromagnetic field, is that the coupling process may also be controlled by varying the relative phase of the input beams [8]. In recent years, much research effort has been dedicated to analyzing the extension of the coupled-mode theory to the case of multiple waveguides [9–16]. In particular, it has been pointed out that, with three or more coupled nonlinear guides, the coupling process is subject to chaotic spatial behavior [9,10,17–19]. On the one hand, this may enhance the sharpness of the switching characteristics, but on the other hand it may introduce undesired instabilities that spoil the proper operation of the array at high powers. The origin of the chaotic instabilities is the lack of a sufficient number of conservation laws (or Manley-Rowe relations), which prevents the possibility of solving the coupled mode equations exactly. The dynamical nature of these instabilities in discrete nonlinear chains has been studied by several authors in a more general context [20,21]. In fact, the propagation in NFA's is described by a set of coupled ordinary differential equations (ODE's) that is known as the standard *discrete nonlinear Schrödinger equation* (DNLSE), since it appears as the natural discretization of the nonlinear Schrödinger equation (NLSE) in the continuum (i.e., partial differential equation). The interest in the dynamics ruled by the DNLSE type of equations goes beyond the field of optics since these equations were also derived in other physical contexts such as, e.g., condensed matter physics, and in particular for polarons [22], or excitons and defects in molecular chains [23] such as, e.g., polyacetylene [24,25]. Recently, the localized modes of modulated waves in a discrete electrical lattice, described by a DNLSE, have been experimentally observed [26].

In this work, we entirely focus our attention on the existence and control of the propagation of stable localized wave packets in waveguide arrays. These spatially localized nonlinear modes of the array originate from the balance between nonlinearity and linear transverse coupling [27]. The existence of different stable self-trapped beams in nonlinear chains is a well known phenomenon in physics [28–37]. Much less is known, however, on the possibility of using these beams for the stable transport of energy across the array [38–45]. So far, the only known localized wave of the bright type, which may move (within a finite range of velocities) in a discrete cubic nonlinear system, is the soliton solution of the integrable so-called Ablowitz-Ladik chain [46,47]. However, optical waveguide arrays are described by the DNLSE, which, on the contrary, is a nonintegrable, so-called *standard*, discretization [46] of the integrable NLSE [48]. Note that, in the context of condensed matter physics, the transport of

*Also at the Dept. of Mathematics and Statistics, University of New Mexico, Albuquerque, NM 87131.

charge neutral magnetic defects across polymer chains is described by moving discrete kinks or dark-soliton-type of wave forms [24,25]. Also in that case, discretization leads to a finite activation energy for enabling the soliton motion, whereas soliton steering across the chain may be achieved by means of an external electric field.

On the other hand, in the continuum NLSE limit it is clear that steering of the spatial solitons may be simply achieved by tilting the incident beam, which entails a linear phase variation across the transverse beam profile at the interface with the nonlinear medium [49–51]. In the discrete case, although the same effect occurs for broad beam distributions [52], it is of interest to understand whether and to what extent the self-trapping or energy localization effect, which is intrinsic to the discreteness of the system [16,37], affects the motion of a tilted discrete soliton. If this is so, as indeed the numerical simulations of Refs. [52,53] have shown, then interesting device applications of the nonlinear array may be conceived. In fact, one may control and scan the output position of the beam by changing its input power by a moderate amount.

The paper is organized as follows. In Sec. II we introduce the governing equation. Section III is aimed at introducing analytical approximate models which permits one to describe in a simple way the discrete self-trapped (DST) modes, which were previously obtained numerically in Ref. [28]. We identify three different operation regimes for a NFA. The first regime (*weak confinement*) is well described by the usual continuum approximation which leads to the NLSE [27]. The second *intermediate* regime is well described by an extended continuum approximation that was introduced in Ref. [53]. This approximation permits one to analyze the behavior of the DST modes by means of a standard variational approximation [54]. The behavior of the DST modes in the third regime of *strong confinement*, may be captured by a truncated three mode description of the array [15]. Finally, we show that a variational approach that retains the discrete nature of the system as well as the evolution of the beam parameters with distance, permits one to reproduce the characteristics of the DST beams in all the mentioned regimes (i.e., to any degree of beam confinement).

Guided by this analysis of DST beams, we consider their mutual interaction in Sec. IV. This is important in view of establishing what are the stable patterns of DST modes that can be stored in the array. We anticipate the conclusion that the preferred states correspond to patterns with a concentration of energy in a few guides only. This result corresponds to a similar property that arises in the non-cw case [55], and it is also interesting for potential technological applications to parallel image processing (e.g., contrast enhancement [56]). We show that very confined DST states are *virtually free of interactions* with neighboring identical states. Therefore these beams can be densely packed into the array.

In Sec. V we analyze in detail the power and phase-controlled steering behavior of the DST beams. Particular attention is devoted to the influence of the degree of mode confinement on the transverse soliton motion. This feature has a large influence on power-dependent beam steering. We reproduce the power dependence of the soliton steering by means of different approximate methods that lead to evolution equations for the beam parameters, in particular the center-of-mass of the beam. We show that the power dependence of the beam velocity is captured by a simple approach that only involves the knowledge of the steady DST profiles. However, an accurate prediction of the actual behavior that is observed in the numerical simulations requires adjustable beam parameters. We compare two predictions of perturbation theory: the one making use of the exact solutions of the Ablowitz-Ladik model [38,43], whereas the other approach involves the discrete variational method. As we shall see, the latter method permits a much more accurate reproduction of the observed phenomena.

II. GOVERNING EQUATIONS

For weakly coupled waveguides, coupled mode theory yields the following equations for the envelope E_n of the electric field in the nth guide:

$$i\partial_Z E_n + \beta_n E_n + C(E_{n+1} + E_{n-1}) + \gamma|E_n|^2 E_n = 0, \quad n = 2, ..., N-1. \quad (1)$$

In Eqs. (1), β_n is the propagation constant of the mode in guide n, C is the linear coupling coefficient, $\gamma = \omega_0 n_2/(cA_{eff})$, n_2 is the nonlinear coefficient, and A_{eff} is the common effective area of the modes. The equations for the guides 1 and N clearly depend on the boundary conditions for the array. In the following we consider the case of periodic arrays (i.e., we apply periodic boundary conditions to the array). We also assume in the following $\beta_n = \beta, n = 1, ..., N$. By introducing the new dimensionless fields $Q_n = \sqrt{\gamma/2C}E_n e^{-i(\beta+2C)Z}$, Eqs. (1) can be transformed into the *standard* DNLSE in the form

$$i\partial_\xi Q_n + (Q_{n+1} + Q_{n-1} - 2Q_n) + 2|Q_n|^2 Q_n = 0, \quad n = 1, ..., N, \quad (2)$$

where $\xi = CZ$ is the normalized propagation distance. The dynamics of DST beams governed by Eqs. (2) will be the object of the following sections.

III. APPROXIMATE ANALYTICAL SOLUTIONS

To date, no exact localized solutions of the standard DNLSE (2) are known. In the work by Scott and MacNeil, bright localized nonlinear modes of the DNLSE were found by numerical methods [28]. In this section, we present different approximate methods that permit to obtain an analytical description of these discrete solitary beams.

A. Continuum approximations

A continuum approximation [61] of the DNLSE (2) may be obtained by introducing $q(x, \xi)$, with $q(x =$

$n, \xi) \equiv Q_n(\xi)$ and by expanding the linear term in a Taylor series around $x = n$. By retaining the first two terms only in this expansion, one obtains the focusing NLSE,

$$iq_\xi + q_{xx} + 2|q|^2 q = 0. \tag{3}$$

We term this the truncated continuum approximation (TCA). Within the limit of validity of this approximation (often referred to as the long wavelength limit) the solution of the discrete problem has the same form and properties as the well known solutions of the completely integrable NLSE [48]. On the other hand, by keeping all the terms in the expansion we obtain [53]

$$iq_\xi + 2|q|^2 q + \frac{1}{\pi}\int_{-\infty}^{+\infty} df \int_{-\infty}^{+\infty} dy \cos(f) q(y,\xi) e^{if(x-y)} = 0. \tag{4}$$

We will term this the complete continuum approximation (CCA). The problem of searching for stationary solutions of Eq. (4) is equivalent to finding the extremal points of the Hamiltonian H of Eq. (4), subject to the constraint (i.e., energy conservation)

$$\int_{-\infty}^{+\infty} dx |q|^2 = \sqrt{\pi} E_0, \tag{5}$$

which is equivalent to

$$\sum_n |Q_n|^2 = \text{const.} \tag{6}$$

It is easy to show that the Hamiltonian H of Eq. (4) reads

$$H = \int_{-\infty}^{+\infty} dx \left[|q|^4 + \frac{1}{2\pi} \times \left(\int_{-\infty}^{+\infty} df \int_{-\infty}^{+\infty} dy \cos(f) q(y,\xi) q^*(x,\xi) e^{if(x-y)} + \int_{-\infty}^{+\infty} df \int_{-\infty}^{+\infty} dy \cos(f) q^*(y,\xi) q(x,\xi) \times e^{-if(x-y)} \right) \right]. \tag{7}$$

In the following, by using the Ritz optimization technique, we limit our search of extremal points of H to a specific form of solution. In particular, since we are dealing with a one dimensional confined beam, we consider the simple standard choice, i.e., the Gaussian trial function [54,57,58]

$$q(x,\xi) = Ae^{-\frac{x^2}{2\alpha^2}}, \quad \alpha > 0, \tag{8}$$

where the amplitude A and the width α will be determined through the minimization of H over the set of Gaussian trial functions. We point out that the Gaussian ansatz permits one to describe satisfactorily the solution of variational problems even in the case for which the asymptotic behavior of the variational solution differs significantly from the exact one, when this is known (see, e.g., Ref. [59]). In the framework of the same variational approach, one has the alternative choice to seek solutions of a more general form which have a closer asymptotic behavior [60]. However, this is often made at the expenses of having a larger number of variational parameters. Here we are aimed at comparing the results of the CCA with Gaussian functions with those arising from other perturbative methods, which will be discussed below. By using the form of $q(x,\xi)$ given in Eq. (8), the reduced Hamiltonian, obtained by computing H, reads

$$\langle H \rangle = \sqrt{\pi} E_0 \left(\frac{E_0}{\alpha\sqrt{2}} + 2e^{-\frac{1}{4\alpha^2}} \right). \tag{9}$$

The α values that give the self-trapped solutions are then obtained by imposing $d\langle H(\alpha)\rangle/d\alpha = 0$. This yields the equation

$$E_0 = \frac{\sqrt{2}}{\alpha} e^{-\frac{1}{4\alpha^2}}. \tag{10}$$

Since in our set of trial functions $E_0 = \alpha|A|^2$, Eq. (10) can be recasted as a simple relation between the amplitude A and the width α of the self-trapped solutions,

$$A^2 = \frac{\sqrt{2}}{\alpha^2} e^{-\frac{1}{4\alpha^2}}. \tag{11}$$

Obviously the obtained results depend on the particular choice of the trial function in Eq. (8). The method can only be as good as the choice of the trial functions permits. In order to verify the domain of validity of the above solutions, a comparison with the numerical solutions in Ref. [28] will be discussed later on.

B. Discrete variational method

A different approximate approach for describing the problem of beam localization is the discrete variational method. In contrast to the previous approach, where the Ritz optimization technique is applied to analyze a (supposedly) equivalent infinite-dimensional dynamical system (4), we may directly proceed to search for discrete solutions of the DNLSE (2) in a restricted subspace, by imposing a suitable ansatz for the beam profile. A procedure of averaging over the discrete transverse dimension leads to a set of coupled ODE's for the evolution of the beam parameters. Therefore this approach permits one to reduce the dimension of the problem from the set of N complex equations [i.e., Eqs. (2)] to a generally much smaller set of equations for the real parameters of the solution. Clearly this method will be of particular advantage whenever the number of waveguides N is large. In order to emphasize this point, we will consider in this subsection the limiting case of an infinite array.

For the DST beam we use as a trial function the following generalization of the one soliton solution of the continuous NLSE,

$$Q_n = a\sqrt{\mu}\,\text{sech}\left[\mu(n-x_0)\right] e^{i\left[\phi + k(n-x_0) + c(n-x_0)^2\right]}. \tag{12}$$

The DST beam (12) is centered at the position x_0, and the fields in adjacent waveguides exhibit a phase difference k. Here we assume that the beam amplitude and width are independent, and we allow for a variation of the beam width μ upon propagation. This is related to the phase front curvature c, which acts as a conjugate variable of the inverse width μ. Note that a reasonable range for the parameters k and c may be deduced from the linear dispersion behavior of the array. In fact, whenever the phase difference between adjacent waveguides reaches the value $k = \pi/2$, the curvature of the dispersion relation changes its sign. This would be equivalent to a loss of diffraction in the continuum case. Since the existence of bright spatial discrete solitons depends on the correct balance between diffraction and nonlinearity, clearly solutions of the type (12) no longer exist, whereas dark discrete solitons may be formed [33]. In fact, as we shall see in the following, the numerical simulations [52,53] show the decay of discrete beams with $k \simeq \pi/2$. Therefore one should consider $|k| \leq 1$ and $|c| \leq 1$ in order to have stability of the solution (12).

The set of equations for the parameters of the beam (12) may be derived from the Lagrangian of the DNLSE (2). Here it is convenient to rewrite the DNLSE by applying the phase transformation $Q_n \rightarrow Q_n \exp(-2i\xi)$ in order to obtain

$$i\partial_\xi Q_n + (Q_{n+1} + Q_{n-1}) + 2|Q_n|^2 Q_n = 0, \qquad n = 1, ..., N. \tag{13}$$

Equation (13) may be derived by means of a variational principle from the Lagrangian

$$L = \sum_{n=-\infty}^{\infty} \frac{i}{2}\left(Q_n^* \frac{dQ_n}{d\xi} - Q_n \frac{dQ_n^*}{d\xi}\right) + Q_{n+1}Q_n^* + Q_{n+1}^* Q_n + |Q_n|^4 . \tag{14}$$

By inserting the ansatz (12) into the Lagrangian (14) and summing up over n we obtain a reduced Lagrangian in terms of the solitary wave parameters,

$$L = -E_0\left[\frac{d\phi}{d\xi} - k\frac{dx_0}{d\xi} + S_1(x_0;\mu)\left(\frac{dk}{d\xi} - 2c\frac{dx_0}{d\xi}\right) + S_2(x_0;\mu)\frac{dc}{d\xi} + h(x_0,k;\mu,c)\right], \tag{15}$$

where the two conserved quantities are the energy E_0,

$$E_0 \equiv \sum_n |Q_n|^2 = a^2\mu \sum_{n=-\infty}^{\infty} \operatorname{sech}^2[\mu(n - x_0)], \tag{16}$$

and the Hamiltonian h,

$$h(x_0,k;\mu,c) = -2\mathrm{Z}(x_0;\mu,c)\cos(k) - E_0\mathrm{N}(x_0;\mu). \tag{17}$$

Here the first term in the Hamiltonian (17) is due to the linear waveguide coupling. Since it represents the discrete analogue to diffraction, in the following we will refer to this term as "discrete diffraction." The second term contains the effect of nonlinearity, and explicitly depends on the total guided energy E_0. We also defined the following quantities:

$$S_j(x_0;\mu) = \frac{\sum_{n=-\infty}^{\infty} (n - x_0)^j \operatorname{sech}^2[\mu(n - x_0)]}{\sum_{n=-\infty}^{\infty} \operatorname{sech}^2[\mu(n - x_0)]}, \tag{18}$$

$$Z(x_0;\mu,c) = \frac{2\pi \sin(c)}{\sinh(\mu)\sinh(\frac{\pi c}{\mu}) \sum_{n=-\infty}^{\infty} \operatorname{sech}^2[\mu(n - x_0)]}, \tag{19}$$

$$N(x_0;\mu) = \frac{\sum_{n=-\infty}^{\infty} \operatorname{sech}^4[\mu(n - x_0)]}{\left[\sum_{n=-\infty}^{\infty} \operatorname{sech}^2[\mu(n - x_0)]\right]^2}. \tag{20}$$

The above sums were normalized so that the total guided energy factors out of the Lagrangian (15). They show a characteristic periodicity with the beam position x_0 because incrementing x_0 by unity can always be compensated for by redefining the summation index n appropriately. Because of the smaller width of $\operatorname{sech}^4(x)$ compared to $\operatorname{sech}^2(x)$ this periodic behavior is most pronounced for the nonlinearity term $N(x_0;\mu)$. Eventually this periodicity will prove responsible for the localization of the solitary wave.

The above formalism permits one to calculate the parameters of a stationary solitary wave. This requires all beam parameters to be independent of ξ. The structure of the Lagrangian (15) implies that the stationary situation always corresponds to an extremum of the Hamiltonian (17). To find an extremum of the diffraction term we have to assume $c = 0$ as well as $k = 0$, which corresponds to a homogeneous phase distribution. Moreover, the periodicity of the sums with respect to x_0 implies to choose either $x_0 = 0$, or $x_0 = 1/2$. This corresponds to a situation where the exciting beam is either centered on a single waveguide, or in the middle between two adjacent waveguides, respectively. Finally, the minimization of the Hamiltonian (17) with respect to μ yields the following explicite expression for the total guided power E_0 as a function of the inverse beam width μ,

$$E_0 = -\left.\frac{\partial \mathrm{Z}(x_0;\mu,0)/\partial\mu}{\partial \mathrm{N}(x_0;\mu)/\partial\mu}\right|_{x_0=0,1/2}. \tag{21}$$

In Sec. III D, we discuss the validity of this equation for the case $x_0 = 0$, when compared with the numerical results of Ref. [28]. On the other hand, both cases $x_0 = 0, 1/2$ will be important for the interpretation of the beam steering results (see Sec. V).

The connection between the variational results from Eq. (21) and the CCA discussed in Sec. III A may be established by applying a continuum approximation to Eq. (21). This can be done easily by replacing the sums in Eqs. (18) by the respective integrals. The minimization of the Hamiltonian with respect to μ leads to

$$E_0 \approx -\frac{6}{\sinh(\mu)}\left[2\mu\coth(\mu)-1\right], \tag{22}$$

which is equivalent to the respective equation (10) derived above in the framework of the CCA, except for the different choice of the trial function. The dependence of E_0 on the position of the beam x_0 is always neglected, whenever a continuum assumption is implied.

C. Three-mode approximation

In the case of strong confinement, that is, whenever a high input energy is essentially coupled to a single waveguide, one may consider a simple approximation which consists in reducing to study the DNLSE (2) for $n = -1, 0, 1$ only. In addition, if we demand symmetry (i.e., $Q_{-1} = Q_1$), the simplified system for the three modes (3WG) takes the form

$$i\frac{dQ_0}{d\xi} + 2Q_1 + 2|Q_0|^2Q_0 = 0, \tag{23}$$
$$i\frac{dQ_1}{d\xi} + Q_0 + 2|Q_1|^2Q_1 = 0.$$

This system was studied in the framework of the coupled-mode equations for the general three-guide array [17,13–15]. Here, we highlight the results relevant to our approximation. Equations (23) have the conserved quantity $S_0 = |Q_0|^2 + 2|Q_1|^2$. This allows for reducing the system to three real degrees of freedom, and convenient variables for the reduced system turn out to be the pseudo-Stokes parameters: $S_1 = |Q_0|^2 - 2|Q_1|^2$, which measures the energy difference, $S_2 = i(Q_1Q_0^* - Q_1^*Q_0)$ and $S_3 = Q_0Q_1^* + Q_0^*Q_1$. These variables show the existence of the second invariant $S_1^3 + 2(S_2^2 + S_3^2) = S_0^2$, which then confine the phase space of the system on the plane. Looking at stationary solutions in the reduced system, one finds different branches (two or four, depending on the value of S_0) [17]. Furthermore, the validity of (23) is based on the assumption that most of the energy is confined in three fibers, and the central one carries a major part. This means that only that branch, if any, where S_1 is positive and increases in S_0, would be consistent with our assumption. Not only does that branch exist, but, as we shall see later, it also follows very closely the numerical solutions in [28]. In Ref. [17] it was shown that this branch was stable in the reduced system. Since in the full array, outside the three waveguides, an exponentially small amount of energy is carried, we believe that this stability feature is preserved and in fact numerical simulations performed along this branch validate this result.

D. Comparison of results

Figure 1 summarizes all the results obtained by means of the various approximations that we have described so far in order to model the self-trapping of discrete solitons. In this figure we plot the normalized input beam energy E_0 [see Eq. (5)] versus E_0/A^2, where A is the input beam amplitude. Note that in the continuous approximation E_0/A^2 also characterizes the beam width (i.e., α), whereas in the discrete system the quantity E_0/A^2 is a measure of the degree of mode localization (or μ^{-1}). In Fig. 1, the diamonds correspond to the numerical results of Ref. [28]. Therefore these data provide a comparative element to estimate the validity of the various approximate methods. The dashed and thin solid lines correspond to the CCA and TCA, respectively. As expected, both give excellent results for large values of E_0/A^2, i.e., whenever the beam profile is wide. However, as the beam confinement decreases, the CCA gives better results until the value $E_0/A^2 \simeq 1.2$ is reached. Beyond this value, discreteness becomes the dominant effect, and the field is essentially confined in three guides. In this regime, the CCA fails and the energy-width relation of the DST beams is very well approximated by the three-waveguide model of the previous subsection (see the dotted line in Fig. 1).

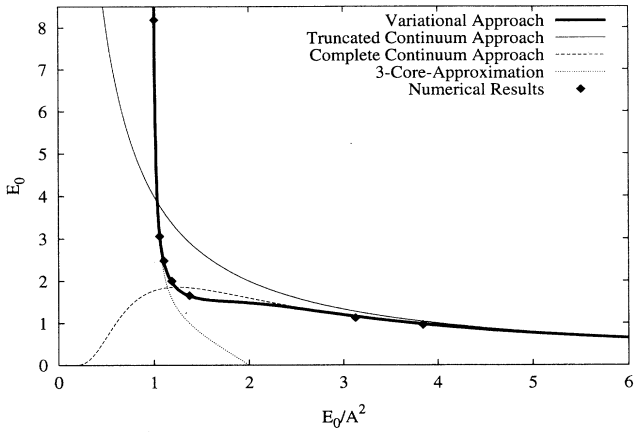

FIG. 1. Plot of the normalized energy E_0 versus E_0/A^2: Diamonds, exact DST solitons (i.e., following Ref. [28]); dashed curve, the TCA; thin solid curve, the CCA; thick solid curve, the variational approach; dotted curve, the three-waveguide approximation.

Finally, the thick solid line in Fig. 1 shows the results of the discrete variational method [see Eq. (21)]. Here we have assumed $x_0 = 0$. In contrast to the previous cases, as can be seen, this approach allows one to always use the same ansatz (12), since this correctly predicts the DST beam properties for both high and low degrees of confinement.

Thus, using different approximations, one may characterize the discrete self-trapped (DST) beams for any value of the input energy. The next step will be the study of DST beams interactions. A quantity which turns to be of convenient use in the next paragraph is the *degree of self-confinement*, which we define as $\mathcal{D}_{SC} \equiv |Q_0|^2/(|Q_0|^2 + 2|Q_1|^2)$.

IV. SOLITON INTERACTIONS

As we shall see DST beams have interesting properties that can be exploited for all-optical storage. The analy-

sis presented in the preceding section allows us to understand, under some approximations, the static properties of the DST beams, but does not elucidate their dynamic properties, such as, for example, their interaction and steering behavior. The interaction problem is addressed in this section, where we make use of both numerical and analytical results, the latter being obtained in the framework of a simple variational analysis.

The degree of self-confinement of self-trapped beams is the pivoting parameter in changing the character of the soliton-soliton interactions. In Figs. 2–6 we present several examples of the interaction behavior of a pair of DST soliton solutions. Throughout the simulations we have used the input condition $Q(n,\xi=0)=f(n-n_1)+f(n+n_2)$, where f is a DST soliton solution of the DNLSE (2) and n_1, n_2 are integer shifts of the initial position of the DST soliton maximum. In order to numerically integrate Eq. (2), we used a variable step fourth-order Runge-Kutta method to solve the N coupled equations with periodic boundary conditions (i.e., circular array).

Figure 2 shows the absence of interactions of two strongly trapped solitons (here $\mathcal{D}_{SC}=0.94$, which corresponds to the third dot from the left in Fig. 1). In Fig. 2(a) we set the soliton separation $\Delta=n_1+n_2=2$, whereas $\Delta=4$ in Fig. 2(b). As can be seen, in this case the DST solitons remain stable even when they are closely packed into the array. Let us see what is the effect of progressively reducing the degree of self-confinement

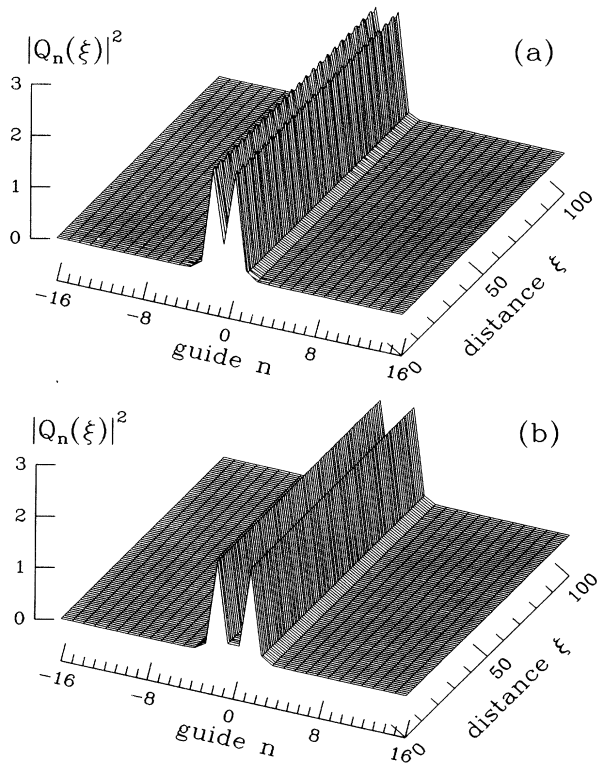

FIG. 3. Weak interactions of two well-confined DST solitons ($\mathcal{D}_{SC}=0.85$). Here $\Delta=2$ (a) and $\Delta=3$ (b).

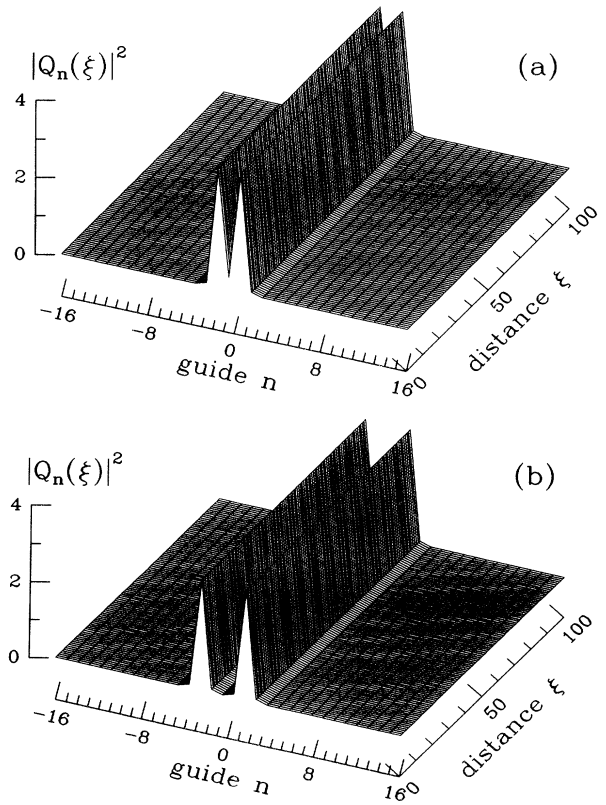

FIG. 2. Absence of interactions of two strongly confined DST solitons ($\mathcal{D}_{SC}=0.94$). Here $\Delta=2$ (a) and $\Delta=4$ (b).

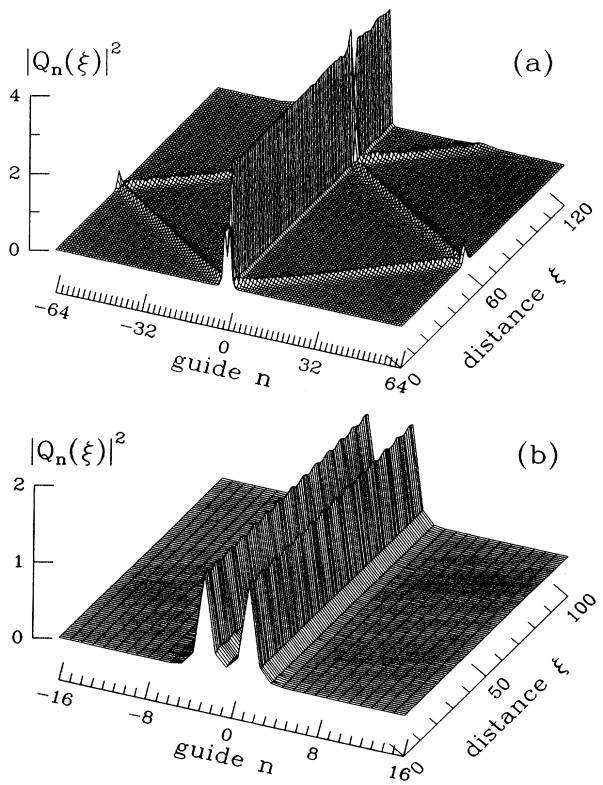

FIG. 4. Interactions of two moderately confined DST solitons ($\mathcal{D}_{SC}=0.75$). Here $\Delta=2$ (a) and $\Delta=4$ (b).

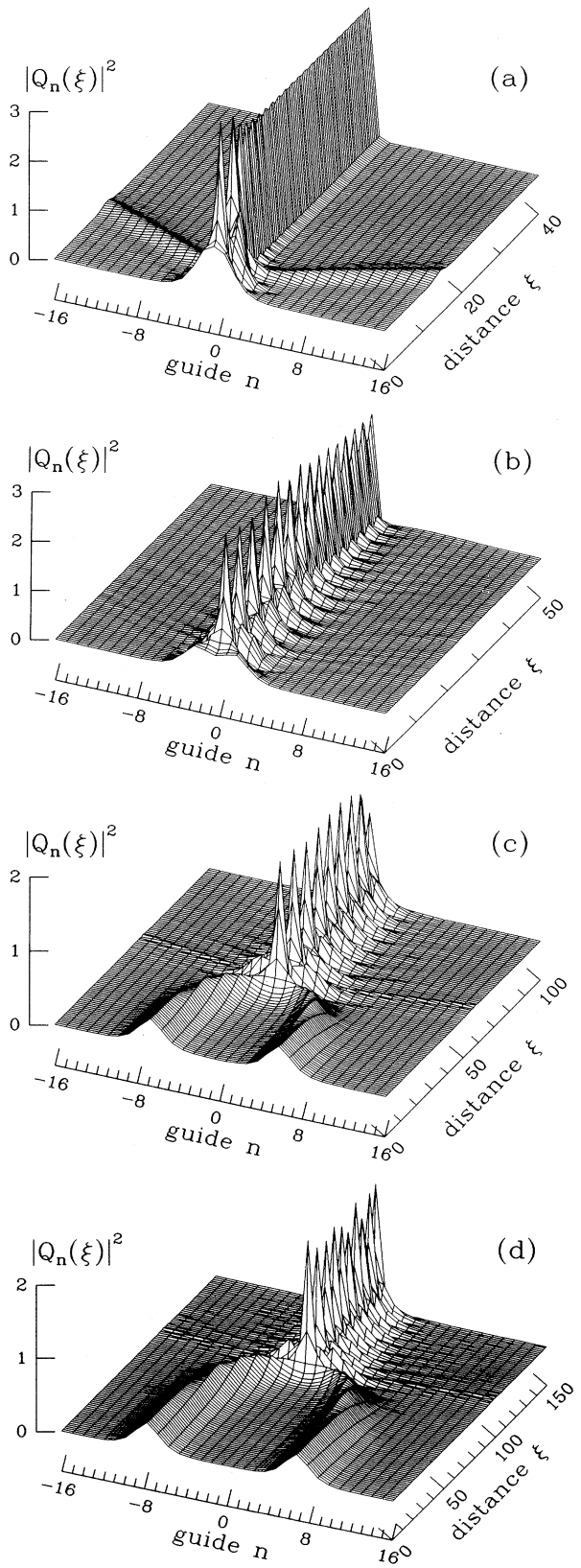

FIG. 5. Collisions of two weakly confined DST solitons ($\mathcal{D}_{SC} = 0.43$). Here $\Delta = 2$ (a), $\Delta = 4$ (b), $\Delta = 12$ (c), and $\Delta = 14$ (d).

$\mathcal{D}_{SC}$. Figure 3 refers to the case $\mathcal{D}_{SC} = 0.85$: with $\Delta = 2$ [see Fig. 3(a)] the solitons remain stable but the interaction produces a weak amplitude oscillation. Whereas for $\Delta = 3$ [see Fig. 3(b)] the two DST solitons generate a spatially stationary pattern. By further reducing the degree of self confinement $\mathcal{D}_{SC}$ below 0.8, relatively strong interactions appear whenever the relative beam separation Δ is smaller than a certain critical value. For example, in Fig. 4(a) we show that the close packing ($\Delta = 2$) of two DST solitons with $D_{SC} = 0.75$ produces the splitting of the field in three DST solitons: two low-amplitude, weakly confined beams travel with opposite velocities backwards and forwards in the array, whereas one compressed, high-amplitude DST beam travels with zero velocity.

Note that, due to the periodic boundary conditions, the low-amplitude beams collide at the end points of the circular array. The particlelike nature of these DST beams, which is a typical property of solitons, is proved by the conservation of the shape and transverse velocity of the beams that emerge from the collision. It is also interesting to observe that the splitting of the initial beam into either a strongly confined, stationary beam, or into low-amplitude, weakly confined rapidly moving beams, suggests that these beams represent the most stable (lowest energy) soliton eigenstates of the DNLSE. On the other hand, Fig. 4(b) shows that by increasing the beam separation up to $\Delta = 4$ the beams maintain their profile and only a weak amplitude oscillation remains. Finally, Fig. 5 displays the interaction behavior of two weakly confined DST beams (here $\mathcal{D}_{SC} = 0.43$). With

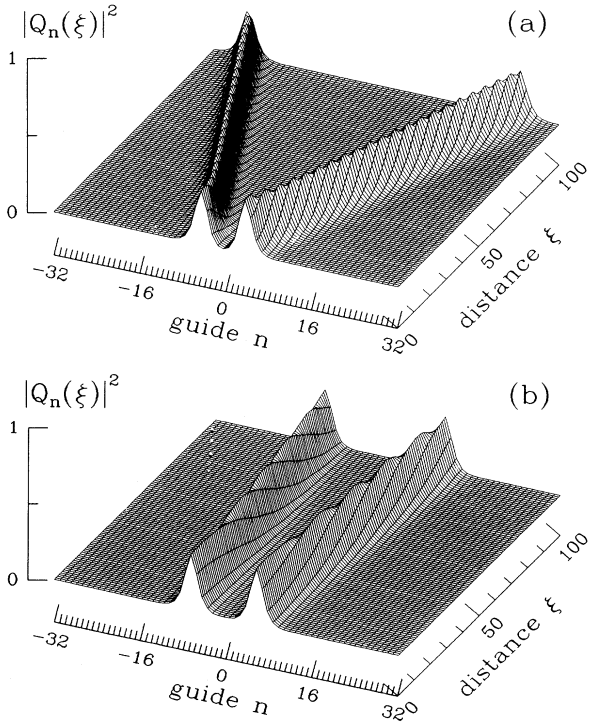

FIG. 6. Repulsion of two π out-of-phase weakly confined DST solitons ($\mathcal{D}_{SC} = 0.43$). Here $\Delta = 8$ (a), and $\Delta = 12$ (b).

$\Delta = 2$ [see Fig. 5(a)] the two strongly overlapping beams produce again three solitons of the type discussed above. Figure 5(a), where $\Delta = 4$, shows that if the initial profile has two distinct peaks, the two low-amplitude moving solitons are no longer generated, and the field self-compresses periodically in space. Thus a kind of higher-order (or breatherlike) discrete soliton is produced. For larger initial beam separations Δ, the propagation of the beams is nearly as in the continuous case, up to the collision point. After the collision, a periodic DST soliton is generated. This is shown by Figs. 5(c,d), that have been obtained for $\Delta = 12$ and $\Delta = 14$, respectively. The weak initial confinement suggests that the behavior that one would predict from the TCA should be observed, at least in the first stage of the propagation. In fact, the two beams collide, as would happen for two NLSE solitons. However, at the coalescence point the spatial compression enhances the role played by discretness and, in contrast with the behavior of the continuum system, the initial state is not periodically recovered. Quite to the contrary, as a result of the interaction an abrupt transition into a strongly trapped periodic breatherlike soliton is observed.

Conversely, whenever the collision is avoided, as for example in the case of two initially π out-of-phase DST beams, the propagation in the weakly confined regime is very similar to that of NLSE solitons. This is shown by Fig. 6, where the repulsion of out-of-phase DST solitons is shown for $\Delta = 8$ [see Fig. 6(a)] and $\Delta = 12$ [see Fig. 6(b)].

We may qualitatively understand the role of discreteness in reducing beam-beam interactions by using simple arguments from perturbation theory. Consistently with TCA, we assume an hyperbolic secant shape for the two beams and set $A = 1/\alpha$. By using the linear dispersion relation of the CCA, soliton perturbation theory [62] yields

$$\frac{d\nu}{d\xi} = 8A^3 e^{-\Delta A}, \qquad \frac{d\Delta}{d\xi} = -4\sin(\nu), \tag{24}$$

where $2\nu = k_1 - k_2$ is the spatial frequency difference between the two beams, and Δ is their peak separation (in the continuous coordinate x). Figure 7 compares the evolution of Δ as a function of ξ, obtained from Eqs. (24) (see solid line) with the evolution ruled by the NLSE (see dashed line) [62]. Here $A = 2$ (corresponding to a degree of self-confinement $\mathcal{D}_{SC} \simeq 0.85$), $\Delta|_{\xi=0} = 2.5$. It is shown that beam coalescence is suppressed by the modification of the linear dispersion relation that is due to discreteness.

V. SOLITON STEERING

Another important property of DST soliton evolution in a nonlinear fiber array deals with their beam steering properties. In the continuous case, beam steering may be trivially achieved by imposing a linear phase variation

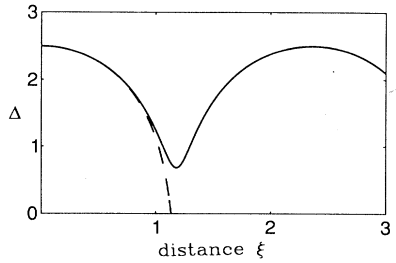

FIG. 7. Evolution of DST beam separation Δ for the continuous NLSE case (dashed line) and from perturbation theory with modified linear dispersion relation owing to discreteness (solid line).

across the transverse profile, which simply corresponds to tilting the input beam. One would naturally expect that the same steering is observed with weakly confined discrete array beams. On the other hand, it is well known from the theory of nonlinear couplers that the nonlinear shift of the propagation constant due to the intensity dependent refractive index tends to decouple otherwise linearly coupled adjacent waveguides through the detuning of their propagation constants. As a consequence, an intense beam that is initially injected into a certain guide remains trapped in it, without transfering any power to the adjacent guides. Therefore, we may argue about the hypothesis for which, for powers above a certain critical value, the localization effect will counterbalance and even cancel the tendency of a tilted beam to obliquely travel across the array. In fact, we have already seen in the preceding section that nonlinear arrays appear to support the stable propagation of two types of localized beams, either broad and moving or narrow and "at rest." In the following, we will try to understand better the transition between these two states by means of both analytical approaches and numerical simulations. Clearly the possibility of controlling, for example, by means of small changes to the initial beam power, the location of the output guide where the beam emerges from the array is very attractive from the point of view of all-optical switching applications.

The transition from the moving to the trapped regime is first shown by the numerical simulations in Figs. 8

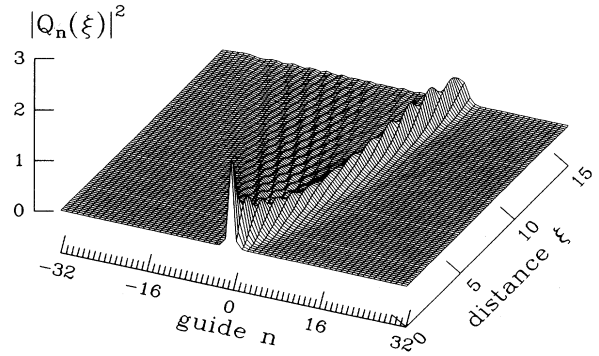

FIG. 8. Moving DST soliton with initial spatial frequency $k = \pi/2$ and $\mathcal{D}_{SC} = 0.85$.

and 9. Here the initial condition was $Q_n(\xi = 0) = f(n)\exp(jkn)$, with $k = \pi/2$ and $\mathcal{D}_{SC} = 0.85$ (see Fig. 8) or $\mathcal{D}_{SC} = 0.94$ (see Fig. 9). As can be seen, the most confined beam is almost unaffected by the initial frequency shift. Whereas the less intense beam generates a soliton that moves down the array with constant speed, at the expense of some energy that is radiated away in the opposite direction when soliton reshaping occurs. Faster solitons (with a fixed offset k) can be generated by launching even broader DST's into the array. As we will discuss in more detail later, we observed the existence of a forbidden gap of velocities as the $\mathcal{D}_{SC}$ is close to 0.9.

This phenomenon may be exploited for all-optical switching by varying either the input energy or the initial phase tilt. In fact, Fig. 10 demonstrates the self-trapping of an initially tilted beam of fixed width and different values of the input energy E_0. Here the input beam was of the form (12) with an inverse transverse width $\mu = 0.75$ and a tilt parameter $k = 0.2$. The beam was initially centered in the wave guide labeled zero. Figure 10 shows the contour plots of the local power levels (relative to the input energy) in the various channels at the output of an array of length $\xi_0 = 10$. As can be seen, at low input energies a broad beam emerges with its center position in the fourth waveguide. At a certain value of threshold energy E_c (here $E_c \simeq 1.5$), the output center position of the beam abruptly switches back to the input waveguide. For energies $E_0 > E_c$, the beam remains trapped in the initial position with an almost fixed value of its transverse width. In the following subsections, we will describe different approximate approaches that lead to the prediction of this effect.

A. Center-of-mass evolution

A simple qualitative understanding of the self-trapping or input power-controlled discrete beam steering may be gained by deriving from the array DNLSE (2) the evolution equation for the center of mass $\bar{n}$ of the beam, which is defined as

$$\bar{n} = \frac{\sum_n |Q_n|^2}{E_0}. \tag{25}$$

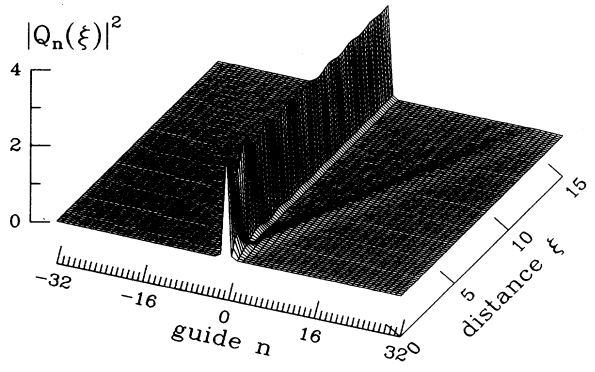

FIG. 9. Trapped DST soliton with initial spatial frequency $k = \pi/2$ and $\mathcal{D}_{SC} = 0.94$.

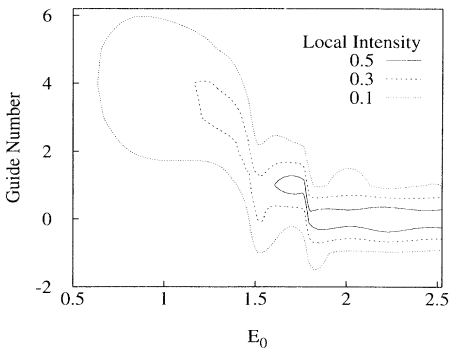

FIG. 10. Contour plot illustrating the self-trapping of a tilted beam of fixed width and different values of the input energy E_0. Parameters are $k = 0.2$, $\mu = 0.75$, and $\xi_0 = 10$.

One obtains from Eqs. (2)–(25)

$$V \equiv \frac{d\bar{n}}{d\xi} = \frac{2}{E_0}\mathrm{Im}\left[\sum_n Q_n Q_{n-1}^*\right]. \tag{26}$$

From this equation one immediately obtains that the velocity V of the center of mass $\bar{n}$ is reduced at high energies. In fact, at low input energies or, equivalently, for a broad input energy distribution among the guides, Eq. (26) may be written as (note that $\mathrm{Im}\{Q_n Q_n^*\} = 0$)

$$\frac{d\bar{n}}{d\xi} = \frac{2}{E_0}\mathrm{Im}\left[\sum_n Q_n(Q_{n-1}^* - Q_n^*)\right] \simeq -\frac{2}{E_0}\int_{-\infty}^{+\infty} QQ_x^* dx = 2\sin(k), \tag{27}$$

where we have set $Q_n = |Q_n|\exp\{ikn\}$. Conversely, for a highly localized beam (i.e., $E_0 >> 1$) one has $|Q_0| \propto \sqrt{E_0}$, $|Q_{\pm 1}| \propto 1/\sqrt{E_0}$, and we obtain instead

$$\frac{d\bar{n}}{d\xi} \simeq \frac{2}{E_0}\mathrm{Im}\{Q_0 Q_1^* + Q_1 Q_0^*\} \simeq \frac{4}{E_0}\sin(k). \tag{28}$$

By comparing Eq. (27) and Eq. (28), one obtains that in the localized regime the velocity V is reduced by the factor $E_0 >> 1$. Therefore the beam steering is inhibited. In order to check this prediction, we may calculate with no approximations, the center-of-mass velocity V from Eq. (26) in the form

$$V = \frac{2}{E_0}\mathrm{Im}\left[\sum_n |Q_n||Q_{n-1}^*|\right]\sin(k), \tag{29}$$

where $|Q_n|$ is the numerically obtained (i.e., "exact") profile of the DST soliton. Figure 11 shows the dependence of the center-of-mass velocity V on the input beam energy E_0, from Eq. (26). Here we considered two different initial tilt angles $k = 0.2, 0.5$. As can be seen, V is rapidly reduced by increasing E_0 up to the critical energy $E_{cr} \simeq 3$. For larger energies, the reduction of V with E_0 is more gradual. Figure 11 shows that the simple center-of-mass equation (26) correctly predicts the

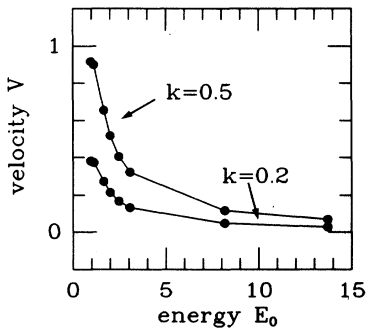

FIG. 11. Prediction for the center-of-mass velocity V from Eq. (26), versus the input beam energy E_0, for different initial tilt angles $k = 0.2, 0.5$.

energy dependence of V. However, the transition between the untrapped and the trapped regimes is not as sharp (in terms of E_0) as in the numerical simulations. In order to demonstrate this point, in Figs. 12–14 we have directly compared predictions of Eq. (26) with the numerical solutions of the array DNLSE (2) with an input tilted DST beam.

Figure 12(a) shows a contour plot of the soliton intensity for a weakly confined beam ($\mathcal{D}_{SC} = 0.43$) and $k = 0.2$, whereas Fig. 12(b) compares the exact (solid

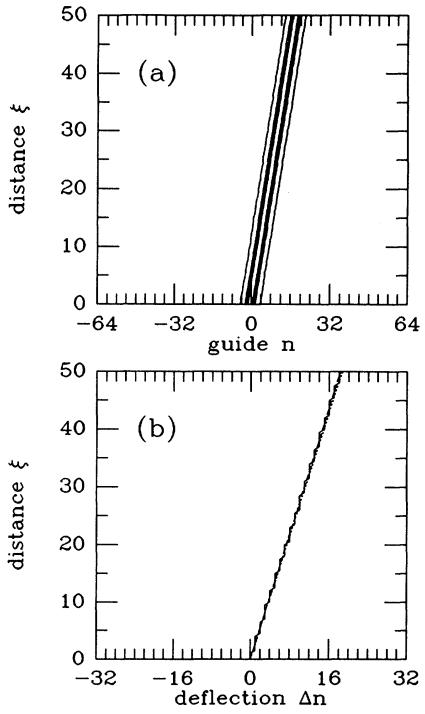

FIG. 12. Comparison between numerical and approximate analytical prediction for the movement of the DST soliton center of mass: (a) contour plot of soliton intensity for a weakly confined beam ($\mathcal{D}_{SC} = 0.43$) and $k = 0.2$; (b) exact (solid line) and approximate (dots) trajectory for the beam center of mass.

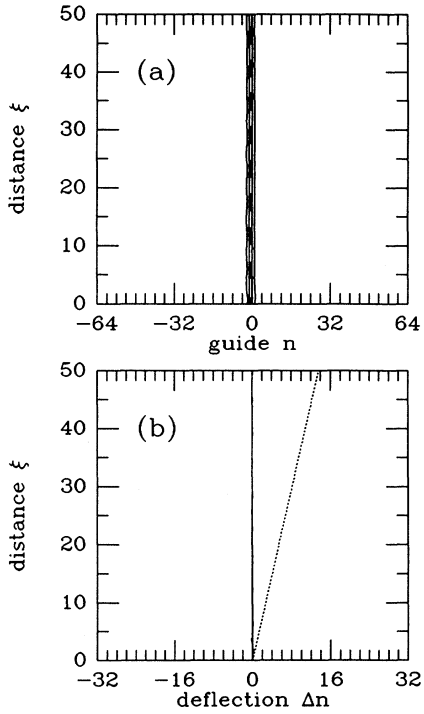

FIG. 13. Same as in Fig. 12, for a beam with an intermediate degree of confinement ($\mathcal{D}_{SC} = 0.75$).

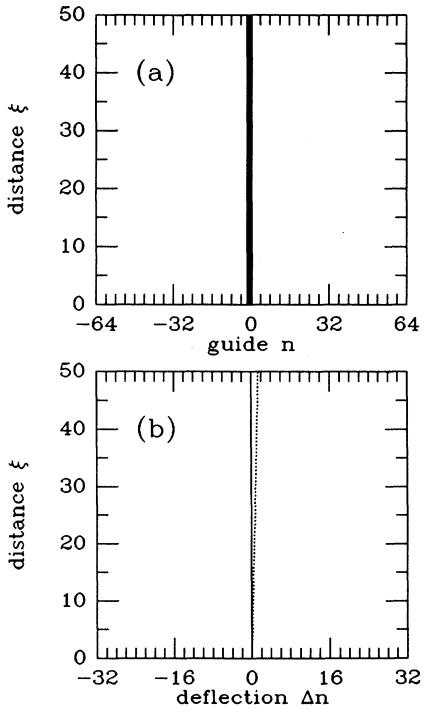

FIG. 14. Same as in Fig. 12, for a beam with a strong degree of confinement ($\mathcal{D}_{SC} = 0.99$).

line) and approximate (dots) trajectories for the beam center of mass $\bar{n}$. In this case there is very good agreement between the two descriptions. On the other hand, Fig. 13 has been obtained for a beam with an intermediate degree of confinement ($\mathcal{D}_{SC} = 0.75$). As can be seen, in this case the numerical solution exhibits self-trapping, whereas the center-of-mass equation (26) does not predict such a drastic reduction for the beam velocity. However, in the limit of high confinements (see Fig. 14), where $\mathcal{D}_{SC} = 0.99$ the simple equation (26) yields nearly complete self-trapping, in agreement with the numerical results. The reason for the discrepancy in the region of intermediate energies (i.e., close to the self-bending threshold E_{cr}) appears to be due to an internal (i.e., in the course of the propagation) dynamics of the initially tilted beam. In other words, the spatial frequency k, the amplitude, and the width of the input beam may change with the distance ξ. Whereas the simple model that we have considered in this subsection clearly assumes that the parameters of the initial beam are maintained unchanged. In the next part of this section, we will discuss two more complex approximate descriptions of the self-steering phenomenon that permit for a dynamical variation of the DST soliton parameters. As we shall see, the best agreement with the numerics is obtained whenever all the parameters of the initial soliton beam are allowed to evolve with distance.

B. Perturbed Ablowitz-Ladik soliton dynamics

A different qualitative understanding of the phenomenon of beam steering along the array can be gained by using soliton perturbation theory applied to the integrable Ablowitz-Ladik nonlinear Schrödinger (ALDNLS) discrete system [47]. We recall here the basic features of this system, which are useful in order to explain the perturbation theory that we are going to employ.

As we mentioned in the Introduction, an integrable discretization scheme of the NLSE, yields the integrable ALDNLS system of equations, which reads

$$i\partial_\xi Q_n + (Q_{n+1} + Q_{n-1} - 2Q_n) + |Q_n|^2(Q_{n-1} + Q_{n+1}) = 0, \quad n = 1, ..., N. \quad (30)$$

The exact one-soliton solution of the ALDNLS is

$$Q_n(z) = \frac{\sinh(\mu)}{\cosh[\mu(n - x_0)]}\exp[ik(n - x_0) + i\alpha], \quad (31)$$

with the following evolution equations for the soliton parameters:

$$\dot{\mu} = \dot{k} = 0,$$
$$\dot{x_0} = \frac{2}{\mu}\sinh(\mu)\sin(k),$$
$$\dot{\alpha} = 2[\cosh(\mu)\cos(k) - 1].$$

The ALDNLS differs from the standard DNLSE only at second order, and only in the nonlinear term. Hence it is natural to rewrite the DNLSE as a perturbed ALDNLS, as follows:

$$i\partial_\xi Q_n + (Q_{n+1} + Q_{n-1} - 2Q_n) + |Q_n|^2(Q_{n-1} + Q_{n+1}) = \epsilon R(Q_n) = |Q_n|^2(Q_{n-1} + Q_{n+1} - 2Q_n), \quad n = 1, ..., N. \quad (32)$$

A soliton perturbation technique for the ALDNLS has been developed in [38]. By means of this method, the evolution of the discrete solitons of Eq. (2) is reduced to the analysis of a system of coupled ODE's, which are well approximated (in the limit $\mu \leq \pi$) by the following system of equations (see Appendix A), which rules the evolution of the parameters $[\mu(\xi), x_0(\xi), k(\xi)]$:

$$\dot{\mu} = 0, \quad (33)$$
$$\dot{x_0} = \frac{2}{\mu}\sinh(\mu)\sin(k), \quad (34)$$
$$\dot{k} = -\frac{2\pi^3\sinh(\mu)^2\sin(2\pi x_0)}{\mu^3\sinh(\frac{\pi^2}{\mu})}. \quad (35)$$

The evolution of the phase α remains uncoupled from the above system. Note that in the limit of small μ's, Eqs. (33)–(35) reduce to

$$\dot{x} = 2\sin(k), \quad (36)$$
$$\dot{k} = 0, \quad (37)$$

which is exactly what one would have obtained in the NLSE limit, by means of the linear dispersion relation of the CCA, as we have shown in the analysis of DST beam interactions in the previous section. Note that Eqs. (36) and (37) do not reveal the existence of a range of parameters in the (k, E_0) plane, in which the DST beam cannot move transversely across the array. Whereas, to the contrary, Eqs. (33)–(35) exhibit such a region, which is in qualitative agreement with the above numerical simulations.

The system of Eqs. (33)–(35) may be simplified by observing that the parameter μ (which here plays the role of the degree of confinement $\mathcal{D}_{SC}$: the higher μ, the higher the degree of self-confinement) is a constant of the motion. This allows for reducing the perturbed evolution of the discrete soliton to a unidimensional nonlinear oscillator, which is described by the conjugate equations

$$\dot{x} = \frac{\partial H}{\partial k}, \quad \dot{k} = -\frac{\partial H}{\partial x}, \quad (38)$$

where $H = H(x, k; \mu)$ is the Hamiltonian

$$H = -\frac{2}{\mu}\sinh(\mu)\cos(k) - \frac{\pi^2\sinh(\mu)^2\cos(2\pi x)}{\mu^3\sinh(\frac{\pi^2}{\mu})}. \quad (39)$$

Hence the study of the motion of a DST beam along the array is now reduced to the analysis of the above simple dynamical system [43]. Following Ref. [43], for example, its fixed points are $k = n\pi, x = \pm m(1/2)$ (for m integer). An interesting feature of the dynamical system (38) and (39) is that the stability of its fixed points does

not depend on the value of the confinement parameter μ. Nevertheless, by changing the value of μ across a certain critical value, say, μ_{crit} ($\mu_{crit} \simeq 3.8$), one may change the topology (and therefore the soliton trapping domain) of the phase plane. In fact, as μ_{crit} is crossed, a switching of the heteroclinic orbit that connects two unstable saddles occurs. This is clearly shown by comparing the phase portraits in Figs. 15 and 16, where $\mu < \mu_{crit}$ and $\mu > \mu_{crit}$, respectively. By inspecting the phase portrait of Fig. 15, where $\mu = 3$, one immediately sees that for certain bands of initial spatial frequency shifts k, the DST may continuously move along the array. In fact, there is a coexistency of regions of forbidden steering (or trapping) and regions where the steering is allowed. Whereas in the phase plane of Fig. 16, where $\mu = 4$, the solitons remain trapped (i.e., execute small amplitude oscillations about their initial position) for any choice of the initial position x and frequency k.

For relatively broad beams, the results of the perturbation analysis [i.e., Eqs. (33)–(39)] are in good agreement with the numerical integration of the DNLSE as far as the prediction of the position of a moving soliton is concerned. On the other hand, for narrow beams (that is, whenever the self-trapping effect becomes important) the perturbation approach based on the perturbed ALDNLS appears to reproduce only in a very qualitative way the propagation properties of DST solitons.

C. Numerical results

Let us take a closer look at the self-trapping phenomenon, which is observed by solving the DNLSE (2), with initial conditions given by the ALDNLS soliton (31). Figure 17 shows some examples of the propagation of moving DST solitons that may be generated in the array. Here the confinement parameter is relatively low, that is,

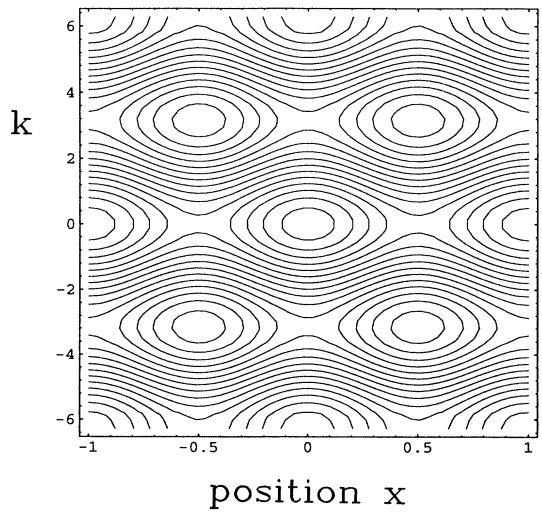

FIG. 15. Phase plane of the Hamiltonian dynamical system obtained through ALDNLS perturbation theory [Eqs. (38 and 39)] for $\mu = 3$.

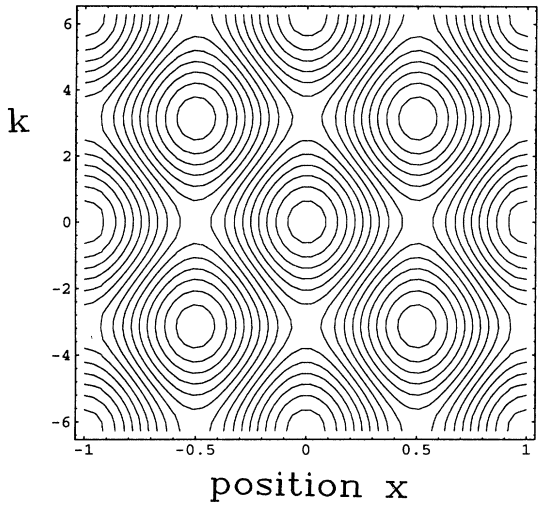

FIG. 16. Phase plane of the Hamiltonian dynamical system obtained through ALDNLS perturbation theory [Eqs. (38 and 39)] for $\mu = 4$.

$\mu = 0.5$. We used different values of the initial spatial frequency (or tilt angle). In Figure 17(a), we have set $k = 0.1$. Correspondingly, the beam slowly moves across the array and its initial shape is retained. Fig. 17(b) shows that the transverse velocity of the discrete soliton grows larger whenever k is increased up to $k = 1$. Again, the input beam profile is maintained during the propagation. On the other hand, Fig. 17(c) shows that whenever the input tilt is increased to the value $k = \pi$ the initially localized beam is destroyed and its energy spreads among the coupled waveguides in a dispersive manner.

In Fig. 18 the confinement parameter of the input beam is increased to $\mu = 1$. In Fig. 18(a) the initial spatial frequency $k = 0.1$. In this case the input profile rapidly reshapes into a narrow and well-confined DST soliton that remains trapped in the central position. Figure 18(b) shows what happens with $k = 1$. The input beam splits into a high-amplitude and oscillating well-confined DST beam and two low-amplitude DST beams that move in opposite directions. Finally, Fig. 18(c) was obtained for $k = 2$; as can be seen, again the propagation of the input beam is strongly dispersive in this case and it is not possible to convey the initial pulse energy into a single moving soliton.

The results in Figs. (17) and (18) indicate that essentially two regimes of propagation exist for DST soliton beams, namely, the moving state for low confinement (i.e., for μ less than a certain critical value, say, μ_{c1}), and the trapped state for $\mu > \mu_{c1}$. In other words, the numerics show that a switching between a moving and a trapped state may be obtained into an array system that is described by the DNLSE by changing the input confinement (which is proportional to the input energy of the beam) with a fixed value of k, and not by varying the input angle k and keeping μ equal to a constant.

In order to find out the value μ_c, one may consider diagrams of the type reported in Fig. 19, where we show the output transmission (which is defined as the output

beam amplitude profile divided by the square root of the input energy E_0), after a propagation distance $\xi_0 = 20$, versus the input confinement parameter μ, for a given value $k = 1$. As can be seen, whenever $\mu < \mu_{c1} \simeq 0.7$ the beam is moving and it emerges at a position that is different from the initial one. Steering of the output position may then be achieved by varying μ below μ_{c1}. For $\mu > \mu_{c1}$, a relatively unstable region exists where the narrow beam may irregularly shift by one position at the output. Finally, for $\mu > \mu_{c2} \simeq 1.3$ the output DST soliton remains stably trapped in the initial position.

Let us consider now the accuracy of the analytical ALDNLS perturbative model [i.e., Eqs. (38) and (39)] in reproducing the above mentioned self-trapping effect. In order to do that, we may trace the shift of the peak of the beam at the array output, as a function of the input confinement parameter μ or, equivalently, of the input beam energy E_0. In each case, we have injected at the input the ALDNLS soliton; therefore larger beam energies correspond to larger confinement factors μ.

Figure 20 illustrates the shift of the position of the output beam peak in a case where the input tilt parameter takes the relatively large value $k = 1$. Here the array length is $\xi_0 = 10$ (dotted line) and $\xi_0 = 20$ (solid line), respectively. As can be seen, the self-trapping effect leads to steering the center position of the output beam in a manner which is almost linear with respect to the energy E_0. For energies larger than the critical value $E_c \simeq 2$, the beam remains stably centered at the initial location.

Figure 21 illustrates some examples of the self-trapping of initial ALDNLS soliton beams in Fig. 20. Here we

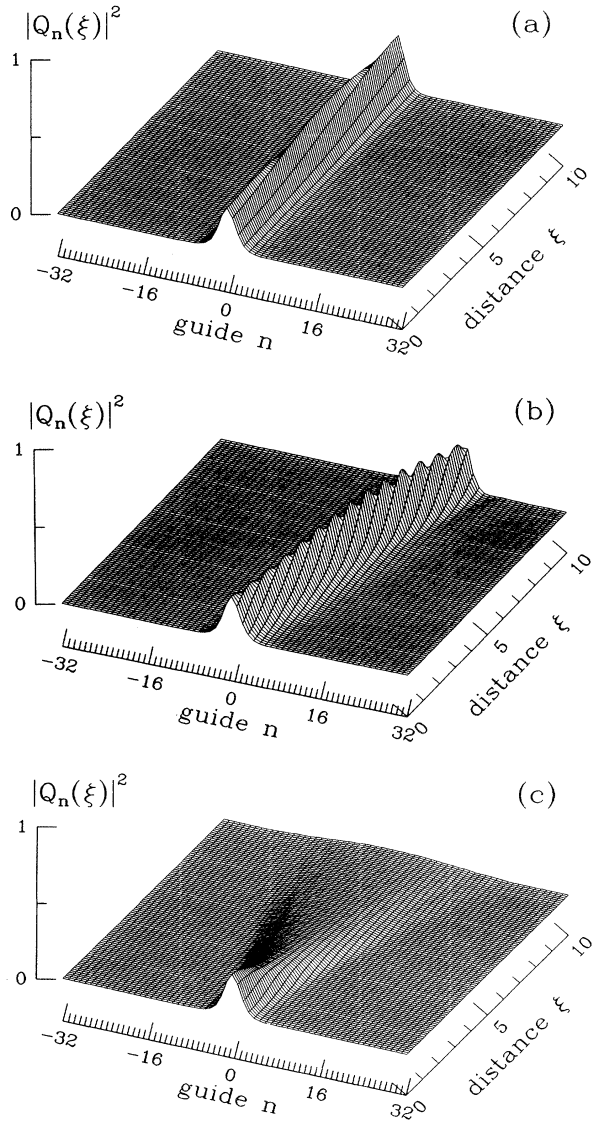

FIG. 17. Moving ALDNLS solitons with the confinement parameter $\mu = 0.5$, and different values of the initial spatial frequency: $k = 0.1$ (a); $k = 1$ (b); $k = \pi$ (c).

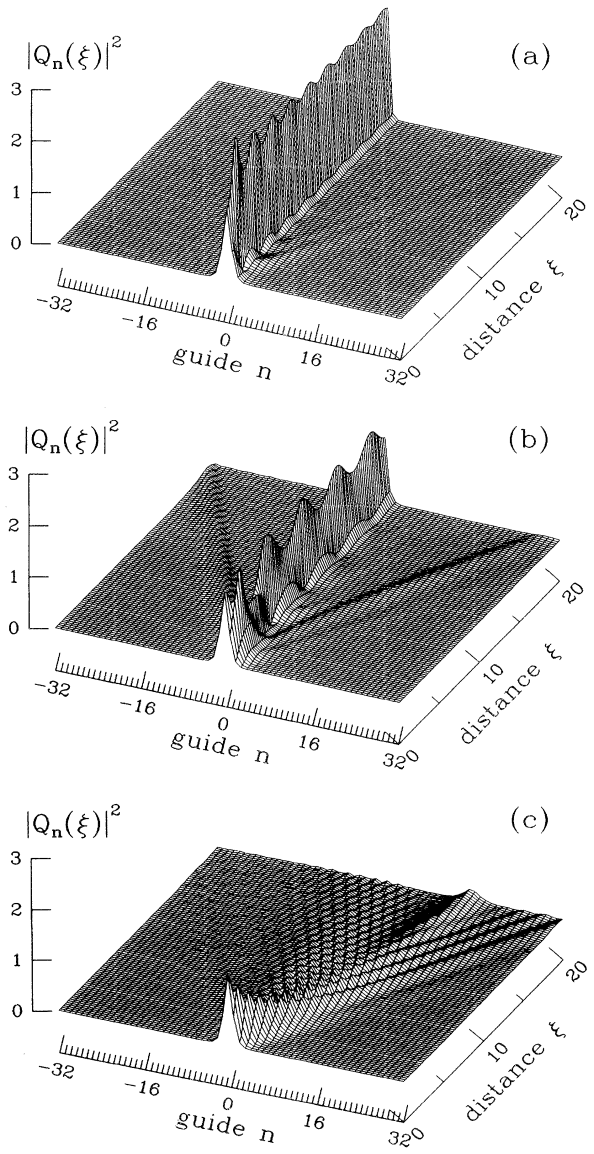

FIG. 18. Moving ALDNLS solitons with the confinement parameter $\mu = 1$, and different values of the initial spatial frequency: $k = 0.1$ (a); $k = 1$ (b); $k = 2$ (c).

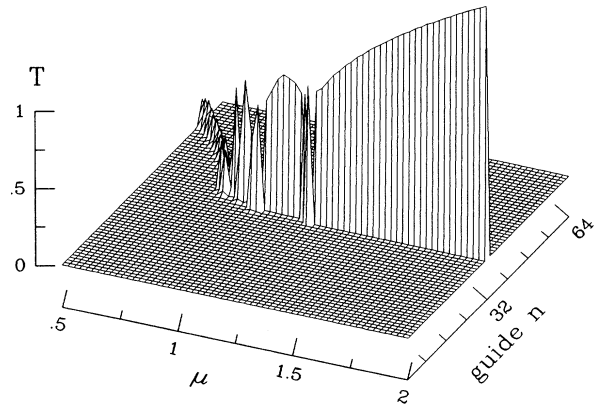

FIG. 19. Output transmission T versus guide number n, for different values of μ, for an array length $\xi_0 = 20$.

show contour plots of the beam intensity for an initial tilt $k = 1$, and different values of the confinement parameter. As can be seen in Fig. 21(a), a weakly confined soliton ($\mu = 0.5$) moves across the array. This corresponds to the region in Fig. 20 below the critical energy E_c. Figure 21(b) has been obtained for $\mu = 0.75$. After the initial transient, the beam location remains approximately fixed. This corresponds to beam energies close to E_c. Finally, in Fig. 21(c) we have set $\mu = 1$, and the beam remains trapped in the input waveguide. Note the emission of energy in the form of radiation on the right-hand side, and a low-power broad moving soliton on the left-hand side of the main beam. The present relaxation of a high-energy beam into a stable nonlinear eigenmode accompanied by the shedding of the extra energy into moving solitons represents a quite general phenomenology. For example, in the continuum limit of the NLSE, one may consider the soliton emission from a linear into a nonlinear waveguide [63].

These effects are substantially similar for smaller tilt parameters k. In fact, Fig. 22 shows the output beam shift for a tilt $k = 0.5$. The array length is again $\xi_0 = 10$ (dotted line) and $\xi_0 = 20$ (solid line). As can be seen, although the absolute value of the shift decreases in a

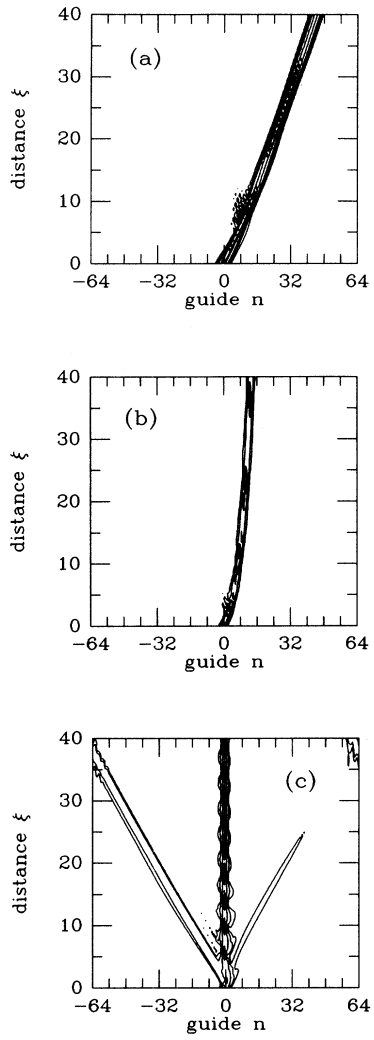

FIG. 21. Self-trapping of ALDNLS solitons. Contour plot of the beam intensity for $k = 1$ and different confinement parameters: (a) $\mu = 0.5$; (b) $\mu = 0.75$; (c) $\mu = 1$.

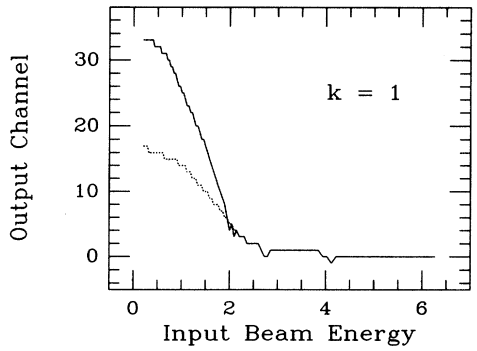

FIG. 20. Peak location of the output beam for a tilt $k = 1$ and the array length $\xi_0 = 10$ (dotted line) and $\xi_0 = 20$ (solid line), for different input beam energies E_0.

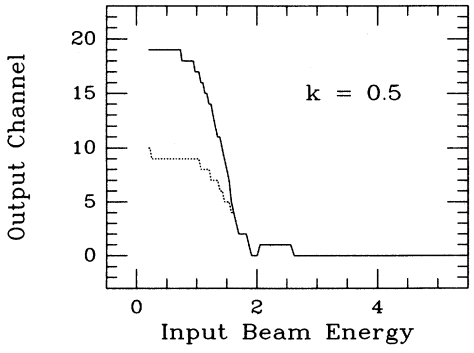

FIG. 22. Peak location of the output beam for a tilt $k = 0.5$ and the array length $\xi_0 = 10$ (dotted line) and $\xi_0 = 20$ (solid line), for different input beam energies E_0.

manner which is proportional to k, *the critical trapping energy remains unchanged with* k.

On the other hand, Fig. 23 shows the energy dependence of the peak location of the output beam when the ALDNLS perturbation theory of Eqs. (38) is used. It reveals that the perturbation theory predicts that the critical trapping energy exhibits a nearly uniform increase whenever the tilt angle k grows larger. Here the array length $\xi_0 = 5$. Moreover, the comparison between Figs. 20–22 and Fig. 23 shows that, although the perturbation theory correctly captures the self-trapping effect as we have seen above, for relatively large values of k's, the perturbative prediction of the trapping energy is much in excess of the numerically observed value E_c. Additionally, Fig. 23 shows that the analytical model of Eqs. (38) predicts that, as the confinement factor μ grows larger than zero, the pulse moves faster across the array, in clear contrast with the behavior of the numerical solutions of the DNLSE (see Figs. 20–22).

Finally, Fig. 24 illustrates the peak location of the output beam vs the input energy E_0, as it is obtained from ALDNLS perturbation theory (dashed line) and from the numerical solutions of the DNLSE (solid line), in the case of a small tilt angle $k = 0.1$. Here the total array length is $\xi_0 = 20$. As can be seen, in this case the shape of the two curves is much more similar than in the previous cases, and the difference between the numerical and perturbative predictions for the trapping energy is reduced to be slightly larger than 2. Better agreements would require smaller values of k, and longer arrays in order to observe a significant shift of the output pulse position.

D. Variational results

In this section we will discuss the performance of the discrete variational method of Sec. III B for predicting the self-steering behavior of DST solitons. The equations of motion for the parameters of the solitary wave (12) are completely determined by the Hamiltonian $h(x_0, k; \mu, c)$ (17), and read

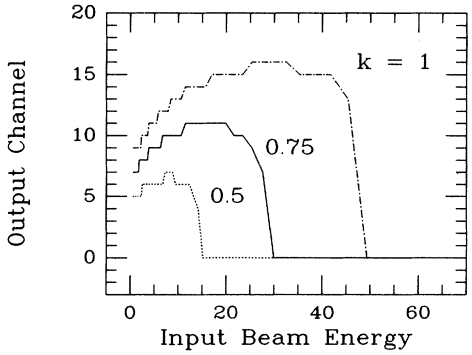

FIG. 23. Peak location of the output beam vs input energy E_0 from ALDNLS perturbation theory with different tilt angles k and the array length $\xi_0 = 5$.

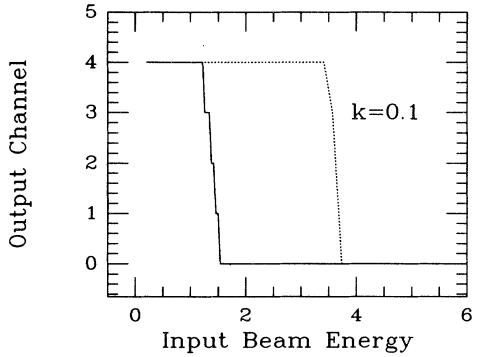

FIG. 24. Peak location of the output beam vs input energy E_0 from ALDNLS perturbation theory (dotted line) and from numerical solutions of the DNLSE (solid line) with a small tilt angle $k = 0.1$, and an array length $\xi_0 = 20$.

$$
\begin{aligned}
\frac{dx_0}{d\xi} &= \frac{\frac{\partial S_2}{\partial \mu}\frac{\partial h}{\partial k} - \frac{\partial S_1}{\partial \mu}\frac{\partial h}{\partial c}}{\frac{\partial S_2}{\partial \mu}\left(1+\frac{\partial S_1}{\partial x_0}\right) - \frac{\partial S_1}{\partial \mu}\left(2S_1+\frac{\partial S_2}{\partial x_0}\right)}, \\
\frac{dk}{d\xi} &= \frac{-\frac{\partial S_2}{\partial \mu}\frac{\partial h}{\partial x_0} + \left(2S_1+\frac{\partial S_2}{\partial x_0}\right)\frac{\partial h}{\partial \mu} - 2c\frac{\partial S_1}{\partial \mu}\frac{\partial h}{\partial c}}{\frac{\partial S_2}{\partial \mu}\left(1+\frac{\partial S_1}{\partial x_0}\right) - \frac{\partial S_1}{\partial \mu}\left(2S_1+\frac{\partial S_2}{\partial x_0}\right)}, \\
\frac{d\mu}{d\xi} &= \frac{\left(1+\frac{\partial S_1}{\partial x_0}\right)\frac{\partial h}{\partial c} - \left(2S_1+\frac{\partial S_2}{\partial x_0}\right)\frac{\partial h}{\partial k}}{\frac{\partial S_2}{\partial \mu}\left(1+\frac{\partial S_1}{\partial x_0}\right) - \frac{\partial S_1}{\partial \mu}\left(2S_1+\frac{\partial S_2}{\partial x_0}\right)}, \\
\frac{dc}{d\xi} &= \frac{-\left(1+\frac{\partial S_1}{\partial x_0}\right)\frac{\partial h}{\partial \mu} + 2c\frac{\partial S_1}{\partial \mu}\frac{\partial h}{\partial k} + \frac{\partial h}{\partial x_0}\frac{\partial S_1}{\partial x_0}}{\frac{\partial S_2}{\partial \mu}\left(1+\frac{\partial S_1}{\partial x_0}\right) - \frac{\partial S_1}{\partial \mu}\left(2S_1+\frac{\partial S_2}{\partial x_0}\right)}.
\end{aligned}
\tag{40}
$$

The evolution equation for the phase ϕ was not included here for shortness. However, this equation may be easily derived from variation of L in Eq. (15) with respect to the energy E_0. Finally, the amplitude a is determined from the conservation of the total guided energy E_0.

Note that in the small energy limit (hence, large values of the beam width μ^{-1}) the derivative $\partial S_2/\partial \mu \propto \mu^{-2}$, whereas the other sums that appear in Eqs. (40) are either constant or directly proportional to μ. Therefore the terms with $\partial S_2/\partial \mu$ will dominate in Eqs. (40), and the equations of motion for the center of mass will decouple from the evolution of the soliton width. Thus one is left with a simple equations of motion for the conjugate pair of position x_0 and phase tilt k,

$$\frac{dx_0}{d\xi} = \frac{\partial h}{\partial k}, \tag{41}$$

$$\frac{dk}{d\xi} = -\frac{\partial h}{\partial x_0}, \tag{42}$$

which is similar to the respective system obtained from the Ablowitz-Ladik model [see Eqs. (38) and (39)]. Similarly to the discussion presented there, most of the physics involved may be elucidated by an investigation of the Hamiltonian h (17). To this purpose we use Eq.

(21) to determine its stationary points, which correspond to the following physical situations: for $x_0 = 0$ we have the soliton centered on a single fiber, while for $x_0 = 1/2$ two adjacent waveguides are equally excited. We have depicted the respective values of the Hamiltonian in Fig. 25. It is clear that $x_0 = 0$ corresponds to an absolute minimum of the Hamiltonian and, hence, is stable. In contrast to the latter case the Hamiltonian exhibits a saddle point for $x_0 = 1/2$, which corresponds to an unstable stationary solution.

Obviously, the value of the Hamiltonian of a moving soliton has to exceed that of the saddle point. Thus the difference between the values for both situations (i.e., $x_0 = 0, 1/2$) gives a measure for the potential barrier, which prevents a beam centered on a single fiber from moving. Note, that each possible initial condition corresponds to one single point in the diagram. In this sense Fig. 25 may be interpreted as a phase diagram which characterizes different types of solutions, as it is indicated by the labels in Fig. 25.

From the height of the potential barrier we may determine the critical phase tilt k_{crit} that a soliton centered on a single guide must have to be able to jump to the next guide. The respective results are depicted in Fig. 26. Obviously, this quantity strongly depends on the power E_0. Localization sets in at a level of $E_0 \approx 1$ and increases rapidly above $E_0 \approx 1.5$. Above a power level $E_0^{crit} = 3.952$ no possible value of the phase tilt will lead to a moving solution. This power level corresponds to a critical inverse beam width $\mu_{crit} = 2.72$ at $x_0 = 0$. This value of the critical inverse beam width has to be compared to the $\mu_{crit} \approx 3.8$, which was determined from the ALDNLS peturbative model. However, the shape of the ALDNLS soliton for $\mu \sim \mu_{crit}$ would lead to a critical energy of $E_0^{crit} \sinh^2 \mu \sim 500$, which differs from the variational result by more than two orders of magnitude. But, nevertheless, even at an energy level as low as 2.5, the critical phase tilt approaches unity and the trial function used to describe the spatial soliton [see Eq. (12)] is no longer reliable.

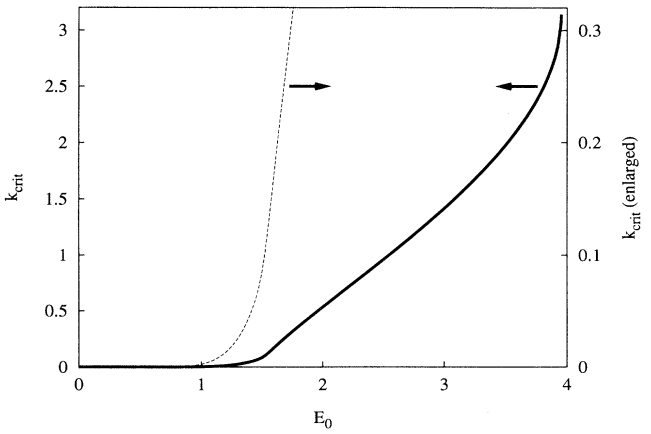

FIG. 26. Critical initial phase tilt k_{crit}, needed to overcome beam localization, as a function of the guided energy E_0 (solid line). Parameters are $x_0 = 0$ and a width corresponding to that of the stationary solution (see Fig. 1). The dashed line shows k_{crit} for $E_0 < 1.5$ on a zoomed scale to highlight the onset of localization.

We applied Eqs. (40) in order to analyze the steering behavior of the beam (12) with the initial tilt $k = 0.2$. Initially the beam is centered at guide number zero. Figure 27 presents a comparison between the numerical results (see the thin line) and the prediction of the variational approach (see the thick line). Here we display the dependence on the input beam energy E_0 of the position of the center of mass of the output beam for an array of length $\xi_0 = 10$. The input beam width was $\mu = 0.75$. As can be seen, using the discrete variational method leads to a much better agreement with the numerical results than using the perturbed ALDNLS model discussed in Sec. V B. It turns out that the improvement

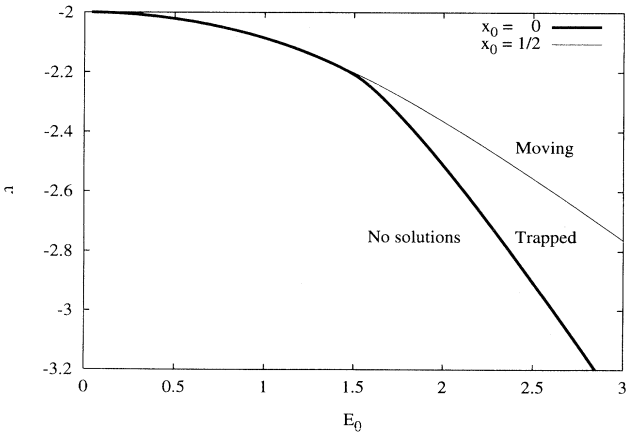

FIG. 25. Values of the Hamiltonian h for stationary solitons centered on a single fiber ($x_0 = 0$) or between two guides ($x_0 = 1/2$), respectively, plotted versus the guided energy E_0. Each possible initial condition corresponds to one point in the plot. Labels indicate the corresponding dynamical behavior.

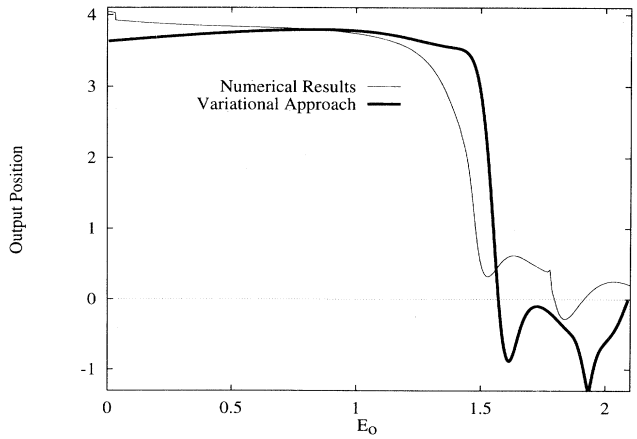

FIG. 27. Comparison between the numerical results (thin line) and those obtained by the variational approach (thick line) for the center of mass of the output beam as a function of the input beam energy E_0. Here $k = 0.2$, $\mu = 0.75$, and $\xi_0 = 10$ (same parameters as in Fig. 10).

of the agreement comes from the fact that in the discrete variational method one allows for independent evolutions of the pulse amplitude and width. Conversely, in the perturbed ALDNLS model the pulse amplitude and width remain fixed along the propagation coordinate ξ, and this cannot account for both width and amplitude changes which accompany the localization effect.

VI. CONCLUSIONS

In this work we compared different analytical descriptions of the self-trapping effect of localized beams in arrays of nonlinear fibers. We have first considered continuum or discrete variational approaches that permit to characterize the field distribution of the beam among adjacent fibers in the various regimes of confinement. Successively, we studied the stability of these DST solitary beams with respect to the interaction with another nearby beam. Finally we analyzed the power-induced control of the transverse motion of DST beams in the array, whenever a linearly varying phase is superimposed onto the input field profile. Indeed we have shown that the speed of this motion may be controlled by varying the degree of self-confinement of the input beam. We found that this energy transport across the array may be completely canceled by the self-trapping effect. This phenomenon may find application for the all-optical controlled steering of the beam at the output of the array. We have compared the merit of different approximate descriptions that model the dynamics of the center of mass of the discrete beam. We found that a simple equation for the center of mass that incorporates the knowledge of the nonlinear eigenmodes or DST solitons of the array pemits to capture in a qualitative manner the power-induced beam steering effect. A more accurate description of the discrete transverse soliton dynamics may be achieved by using a discrete variational approach that yields evolution equations for a small number of parameters of the beam.

ACKNOWLEDGMENTS

This work was carried out in the frame of European Collaboration in Science and Technology (COST) project No. 241. The work of A.B.A. and C.D.A. was supported by U.S. Department of Energy Grant No. DE-FG03-93ER25163, and AFOSR Grant No. F49620-94-1-0007. The work of S.T. and S.W. was carried out in the framework of the agreement between Fondazione Ugo Bordoni and the Italian Post and Telecommunications Administration. T.P. and F.L. would like to acknowledge financial support from "Deutsche Forschungsgemeinschaft," Germany, in the framework of the program on optical signal processing.

APPENDIX A: DISCRETE PERTURBATION THEORY

In this section we outline, for sake of completeness, the general method to obtain the evolution equations for the soliton parameters, in the framework of the adiabatic approximation of soliton perturbation theory based on the inverse scattering transform of the Ablowitz-Ladik system. In general, for a perturbed ALDNLS of the form

$$i\partial_\xi Q_n + (Q_{n+1} + Q_{n-1} - 2Q_n) + |Q_n|^2(Q_{n-1} + Q_{n+1}) = \epsilon R(Q_n)\ , \quad n = 1, ..., N, \tag{A1}$$

one obtains the following equations for the soliton parameters $[\mu(\xi), x_0(\xi), k(\xi)]$:

$$\dot{\mu} = \epsilon \sinh(\mu) \sum_{n=-\infty}^{\infty} \frac{\cosh[\mu(n - x_0)]}{\cosh[\mu(n + 1 - x_0)]\cosh(n - 1 - x_0)} \times \mathrm{Im}\{R(Q_{ns})\exp[-ik(n - x) - i\alpha]\}, \tag{A2}$$

$$\dot{x_0} = \frac{2}{\mu}\sinh(\mu)\sin(k) + \epsilon \frac{\sinh(\mu)}{\mu} \times \sum_{n=-\infty}^{\infty} \frac{(n - x_0)\cosh[\mu(n - x_0)]}{\cosh[\mu(n + 1 - x_0)]\cosh(n - 1 - x_0)} \times \mathrm{Im}\{R(Q_{ns})\exp[-ik(n - x) - i\alpha]\}, \tag{A3}$$

$$\dot{k} = -\epsilon \sinh(\mu) \sum_{n=-\infty}^{\infty} \frac{\tanh[\mu(n - x_0)]\cosh[\mu(n - x_0)]}{\cosh[\mu(n + 1 - x_0)]\cosh(n - 1 - x_0)} \times \mathrm{Re}\{R(Q_{ns})\exp[-ik(n - x) - i\alpha]\}. \tag{A4}$$

When applying Eqs. (A4) to a specific perturbation, it is useful to employ the Poisson formula

$$\sum_{n=-\infty}^{\infty} f(na) = \int_{n=-\infty}^{\infty} \frac{dx}{a} f(x) \left[1 + 2\sum_{s=1}^{\infty} \cos\left(\frac{2\pi s x}{a}\right)\right]. \tag{A5}$$

Then Eqs. (33)–(35) are obtained by retaining only the first harmonic (i.e., $s = 1$) of Eq. (A5).

[1] H. A. Haus and L. Molter-Orr, IEEE J. Quantum Electron. **QE-19**, 840 (1983).
[2] D. B. Mortimore and J. W. Arkwright, Appl. Opt. **29**, 1814 (1990).
[3] D. B. Mortimore and J. V. Arkwright, Appl. Opt. **30**, 650 (1991).
[4] W. M. Henry and A. Travis, Opt. Quantum Electron. **24**, 833 (1992).
[5] K. Okamoto, H. Takahashi, S. Suzuki, A. Sugita, and Y. Ohmori, Electron. Lett. **27**, 774 (1991).
[6] S. M. Jensen, IEEE J. Quantum Electron. **QE-18**, 1580 (1982).

[7] A. A. Maier, Sov. J. Quantum Electron. **12**, 1490 (1983).
[8] B. Daino, G. Gregori, and S. Wabnitz, J. Appl. Phys. **58**, 4512 (1985).
[9] S. Trillo and S. Wabnitz, J. Opt. Soc. Am. B **5**, 483 (1988).
[10] N. Finlayson and G. I. Stegeman, Appl. Phys. Lett. **56**, 2276 (1990).
[11] D. J. Mitchell, A. W. Snyder, and Y. Chen, Electron. Lett. **26**, 76 (1990); **26**, 1164 (1990).
[12] C. Schmidt-Hattenberger, U. Trutschel, and F. Lederer, Opt. Lett. **16**, 294 (1991).
[13] C. Schmidt-Hattenberger, U. Trutschel, R. Muschall, and F. Lederer, Opt. Commun. **82**, 461 (1991).
[14] C. Schmidt-Hattenberger, U. Trutschel, R. Muschall, and F. Lederer, Opt. Commun. **89**, 473 (1992).
[15] C. Schmidt-Hattenberger, R. Muschall, U. Trutschel, and F. Lederer, Opt. Quantum Electron. **24**, 691 (1992).
[16] M. I. Molina, W. D. Deering, and G. P. Tsironis, Physica D **66**, 135 (1993).
[17] K. W. DeLong, J. Yumoto, and N. Finlayson, Physica D **54**, 36 (1991).
[18] N. Finlayson, K. J. Blow, L. J. Bernstein, and K. W. DeLong, Phys. Rev. A **48**, 3863 (1993).
[19] D. Henning, H. Gabriel, M. F. Jørgensen, P. L. Christiansen, and C. B. Clausen, Phys. Rev. E **51**, 2870 (1995).
[20] J. Carr and J. C. Eilbeck, Phys. Lett. A **109**, 201 (1985).
[21] D. W. McLaughlin and C. M. Schober, Physica D **57**, 447 (1992).
[22] T. Holstein, Ann. Phys. **8**, 325 (1959).
[23] A. S. Davydov and N. I. Kislukha, Phys. Status Solidi (B) **59**, 465 (1973).
[24] W. P. Su, J. R. Schrieffer, and A. J. Heeger, Phys. Rev. Lett. **42**, 1698 (1979); Phys. Rev. B **22**, 2099 (1980).
[25] H. Takayama, Y. R. Lin-Liu, and K. Maki, Phys. Rev. B **21**, 2388 (1980).
[26] P. Marquii, J. M. Bilbault, and M. Remoissenet, Phys. Rev. E **51**, 6127 (1995).
[27] D. N. Christodoulides and R. I. Joseph, Opt. Lett. **13**, 794 (1988).
[28] A. C. Scott and L. MacNeil, Phys. Lett. A **98**, 87 (1983).
[29] J. C. Eilbeck, P. S. Lomdahl, and A. C. Scott, Physica D **16**, 318 (1985).
[30] A. J. Sievers and S. Takeno, Phys. Rev. Lett. **61**, 970 (1988).
[31] J. B. Page, Phys. Rev. B **41**, 7835 (1990).
[32] S. Takeno and K. Hori, J. Phys. Soc. Jpn. **60**, 947 (1991).
[33] Yu. S. Kivshar, Opt. Lett. **18**, 1147 (1993).
[34] Yu. S. Kivshar, Phys. Lett. A **173**, 172 (1993).
[35] Yu. S. Kivshar, Phys. Rev. Lett. **70**, 3055 (1993).
[36] M. I. Molina and G. P. Tsironis, Physica D **65**, 267 (1993).
[37] L. J. Bernstein, K. W. DeLong, and N. Finlayson, Phys. Lett. A **181**, 135 (1993).
[38] A. A. Vakhnenko and Yu. B. Gaididei, Theor. Math. Phys. **68**, 873 (1986).
[39] S. Takeno and K. Hori, J. Phys. Soc. Jpn. **59**, 3037 (1990).
[40] R. Scharf and A. R. Bishop, Phys. Rev. A **43**, 6535 (1991).
[41] S. R. Bickham, A. J. Sievers, and S. Takeno, Phys. Rev. B **45**, 10344 (1992).
[42] Yu. S. Kivshar and D. K. Campbell, Phys. Rev. E **48**, 3077 (1993).
[43] Ch. Claude, Yu. S. Kivshar, O. Kluth, and K. H. Spatschek, Phys. Rev. B **47**, 14 228 (1993).
[44] D. Cai, A. R. Bishop, and N. Gronbech-Jensen, Phys. Rev. Lett. **72**, 591 (1994).
[45] D. Cai, A. R. Bishop, N. G. Gronbech-Jensen, and B. A. Malomed, Phys. Rev. E **50**, R694 (1994).
[46] M. J. Ablowitz and P. A. Clarkson, *Solitons, Nonlinear Evolution Equations and Inverse Scattering*, London Mathematical Society, Lecture Note Series, Vol. 149 (Cambridge University Press, Cambridge, 1991).
[47] M. J. Ablowitz and J. F. Ladik, J. Math. Phys. **17**, 1011 (1976).
[48] V. E. Zakharov and A. B. Shabat, Zh. Eksp. Teor. Fiz. **61**, 118 (1971) [Sov. Phys. JETP **34**, 62 (1972)].
[49] P. V. Mamyshev, A. Villeneuve, G. I. Stegeman, and J. S. Aitchinson, Electron. Lett. **30**, 726 (1994).
[50] A. T. Ryan and G. P. Agrawal, Opt. Lett. **18**, 1795 (1993).
[51] X. D. Cao, D. D. Meyerhofer, and G. P. Agrawal, J. Opt. Soc. Am. B **11**, 2224 (1994).
[52] W. Krolikowski, U. Trutschel, M. Cronin-Golomb, and C. Schmidt-Hattenberger, Opt. Lett. **19**, 320 (1994).
[53] A. B. Aceves, C. De Angelis, S. Trillo, and S. Wabnitz, Opt. Lett. **19**, 332 (1994).
[54] D. Anderson, Phys. Rev. A **27**, 3135 (1983).
[55] A. B. Aceves, C. De Angelis, A. M. Rubenchik, and S. K. Turitsyn, Opt. Lett. **19**, 329 (1994).
[56] W. J. Firth and B. A. Samson, *Digest of Nonlinear Guided-Wave Phenomena (NLGW) Conference 1993, September 20-22, Cambridge, UK* (Optical Society of America, Washington, D.C., 1993), p. 82.
[57] R. Courant and D. Hilbert, *Methods of Mathematical Physics* (Interscience, New York, 1953) Vol. 1.
[58] R. A. Sammut and C. Pask, J. Opt. Soc. Am. B **8**, 395 (1991).
[59] V. V. Steblina, Y. S. Kivshar, M. Lisak, and B. A. Malomed, Opt. Commun. **118**, 345 (1995).
[60] K. Hayata, M. Koshiba, and M. Suzuki, Electron. Lett. **22**, 1070 (1986).
[61] S. Kawakami and H. A. Haus, J. Lightwave Tech. **LT-4**, 160 (1986).
[62] V. I. Karpman and V. V. Solov'ev, Physica D **3**, 487 (1981).
[63] E. M. Wright, G. I. Stegeman, C. T. Seaton, J. V. Moloney, and A. D. Boardman, Phys. Rev. A **34**, 4442 (1986).